



## Efficient photoelectrochemical water splitting over $\text{Co}_3\text{O}_4$ and $\text{Co}_3\text{O}_4/\text{Ag}$ composite structure



Tiantian Hong<sup>a</sup>, Zhifeng Liu<sup>a,\*</sup>, Xuerong Zheng<sup>b</sup>, Jing Zhang<sup>a</sup>, Lu Yan<sup>a</sup>

<sup>a</sup> School of Materials Science and Engineering, Tianjin Chengjian University, 300384, Tianjin, China

<sup>b</sup> School of Materials Science and Engineering, Key Laboratory of Advanced Ceramics and Machining Technology of Ministry of Education, Tianjin University, 300072, Tianjin, China

### ARTICLE INFO

#### Article history:

Received 27 June 2016

Received in revised form 16 August 2016

Accepted 24 September 2016

Available online 26 September 2016

#### Keywords:

$\text{Co}_3\text{O}_4$

Nanowires

Nanolayers

Ag

Photoelectrochemical water splitting

### ABSTRACT

In this paper,  $\text{Co}_3\text{O}_4$  with different morphologies of nanowires (NWs) and nanolayers (NLs) and Ag modified  $\text{Co}_3\text{O}_4$  are prepared on ITO substrate via a facile and low-cost hydrothermal successfully.  $\text{Co}_3\text{O}_4/\text{Ag}$  composite structure served as photocathode applied in photoelectrochemical (PEC) water splitting presents efficient PEC activity for the first time. The enhanced optical and photoelectrochemical performance are characterized, the role of Ag nanoparticles is discussed. The photocurrent densities of  $\text{Co}_3\text{O}_4/\text{Ag}$  NWs and  $\text{Co}_3\text{O}_4/\text{Ag}$  NLs are up to  $-4.73 \text{ mA cm}^{-2}$  and  $-4.26 \text{ mA cm}^{-2}$ , respectively. The improved PEC performance is attributed to a high light-harvesting efficiency, an expanded photoresponse range, accelerated holes mobility and increased interfacial photoelectrons transport of Ag nanoparticles.

© 2016 Elsevier B.V. All rights reserved.

## 1. Introduction

Efficient utilization of solar energy can relieve lots of energy and environmental concerns, as the solar energy radiating the earth is exceeding the global human energy consumption far surpasses [1,2]. Over water splitting using sunlight illumination has received extensive attention for the production of hydrogen from water [3–5]. Since the first discovery of photo-assisted electrochemical water oxidation using  $\text{TiO}_2$  single-crystal photoelectrode by Honda-Fujishima in the early 1970s [6], photoelectrochemical (PEC) water splitting based on semiconductor materials has been investigated extensively [7,8]. Nowadays, solar hydrogen plays a key role in the sustainable energy societies due to its properties of storable and transportable, as well as it can be directly converted into electricity. To date, metal oxide semiconductor materials have been applied in the PEC water splitting for hydrogen evolution. Among the metal oxide semiconductors, n-type metal oxides, such as  $\text{ZnO}$ ,  $\text{TiO}_2$  and  $\text{WO}_3$  have occupied a large proportion of the literature in the area because these materials are naturally abundant, thermally and chemically stable as well as easy to process [9–13]. However, these n-type metal oxide semiconductors served as photoanodes were used to drive water oxidation for oxygen gen-

eration in the PEC process while hydrogen evolution took place at the counter electrode. Hence, the exploitation of p-type oxide semiconductors photocathodes for direct hydrogen evolution becomes a significant challenge [14].

Cobaltic oxide ( $\text{Co}_3\text{O}_4$ ) is a typical and environmentally friendly p-type metal oxide, which has been extensively used in lithium batteries, super capacitors catalysts and photoelectrochemical devices because of its excellent physical-chemical properties [15–19].  $\text{Co}_3\text{O}_4$  with an appropriate optical band gap of 2.07 eV that could harvest visible light has been used as a photocathode in the PEC procedure to produce hydrogen. Nevertheless, the main limitation of pure  $\text{Co}_3\text{O}_4$  in PEC process is the slow separation of photo-induced electron-hole pairs [20]. And now the catalytic performance of metal oxide semiconductors can be improved largely by increasing the surface area through controlling the morphology of nanolayers and nanowires, which facilitate the separation of photo-induced electron-hole pairs within the material [21]. Furthermore, loading of appropriate noble metallic nanoparticles as an electron trap is in favor of improving the PEC performance dramatically [22–25]. Among lots of different noble metals, Ag is unique in its stability that does not undergo corrosion in the photoreaction process, and it also acted as reduction active sites, which capture the photogenerated electrons from the surface of semiconductor effectively [26]. Therefore, the incorporation of conductive Ag species can obtain the higher performance over pure  $\text{Co}_3\text{O}_4$  cathode.

\* Corresponding author.

E-mail address: [tjulzf@163.com](mailto:tjulzf@163.com) (Z. Liu).

Despite the  $\text{Co}_3\text{O}_4$  with p-type behavior has been mostly served as catalyst and co-catalyst that applied in the oxygen evolution reaction, but there are only few researches on cobaltosic oxide for photoelectrochemical hydrogen evolution reaction [27,28]. In this article, we have firstly synthesized a series of  $\text{Co}_3\text{O}_4$  metal oxides with different morphologies of nanolayers and nanowires on ITO substrate through the hydrothermal and annealing process. Additionally, metal Ag nanoparticles were decorated on  $\text{Co}_3\text{O}_4$  to form a  $\text{Co}_3\text{O}_4/\text{Ag}$  composite structure. The  $\text{Co}_3\text{O}_4$  and  $\text{Co}_3\text{O}_4/\text{Ag}$  were utilized as the photocathodes in the PEC system, respectively. The  $\text{Co}_3\text{O}_4/\text{Ag}$  exhibits enhanced PEC performance compared to the pure  $\text{Co}_3\text{O}_4$ , in particular, the  $\text{Co}_3\text{O}_4/\text{Ag}$  composite structure with  $\text{Co}_3\text{O}_4$  nanowire morphology presents the most excellent PEC activity, exhibiting a high photocurrent and the value was up to  $4.73 \text{ mA cm}^{-2}$ . The higher photocatalytic property in PEC water splitting was obtained due to the following factors: low-dimension  $\text{Co}_3\text{O}_4$  structure has a high specific surface area, which provides a direct pathway for facile electron transfer, providing an excellent substrate for Ag NPs loading and PEC hydrogen generation. The nanostructures can efficient capture the incident light by internal multiscattering. Moreover, the existence of Ag nanoparticles can accelerate interfacial electrons transport, which enhances the charge separation efficiently and suppress the recombination of photo generated electron-hole pairs.

## 2. Experiment

### 2.1. The preparation of $\text{Co}_3\text{O}_4$

The  $\text{Co}_3\text{O}_4$  was synthesized on the indium tin oxide (ITO) substrates combing hydrothermal with heat treatment process. Firstly, the ITO glass was ultrasonically rinsed in acetone, isopropyl alcohol and ethanol for 0.5 h, respectively. Then the substrates were transformed into teflon-lined stainless steel autoclave containing 0.05 M cobalt nitrate and urea with equal concentration. The autoclave was sealed and maintained at  $100^\circ\text{C}$  for various time and then cooled down to room temperature. Finally,  $\text{Co}_3\text{O}_4$  was obtained after heat treatment of as-prepared samples in muffle at  $430^\circ\text{C}$  for 3 h.

### 2.2. The preparation of $\text{Co}_3\text{O}_4/\text{Ag}$

The ITO substrate coated with  $\text{Co}_3\text{O}_4$  sample was immersed in a mixture solution containing 1 mM silver nitrate and 0.7 mM sodium citrate at  $100^\circ\text{C}$  for 2 h. Afterwards, the  $\text{Co}_3\text{O}_4/\text{Ag}$  was rinsed with deionized water and dried in air.

### 2.3. Characterization

Morphology of the products was examined by HITACHI S-4800I field emission scanning electron microscope (FE-SEM) and HITACHI H-7650 transmission electron microscopy (TEM) operated at an accelerating voltage of 100 kV. Optical absorbance of the electrodes was tested by DU-8B UV-vis double-beam spectrophotometer. The photoelectrochemical measurement of the samples was conducted in a three-electrode configuration, which consist of the obtained samples as working electrode, a platinum as counter electrode and a saturated Ag/AgCl as reference electrode. The electrolyte was prepared by 1 M KOH aqueous solution for water splitting experiment. Electrochemical impedance spectroscopy (EIS) of the products was characterized using an electrochemical workstation. The photocurrent density was measured under AM 1.5 ( $100 \text{ mW cm}^{-2}$ ) illumination.

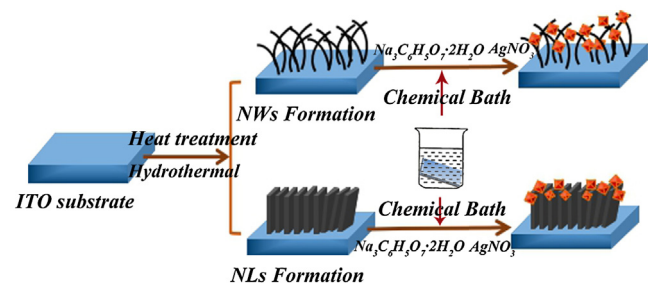


Fig. 1. Synthetic procedure of  $\text{Co}_3\text{O}_4/\text{Ag}$  composite structure.

## 3. Results and discussion

An illustrative synthetic process of  $\text{Co}_3\text{O}_4/\text{Ag}$  is summarized in Fig. 1. Firstly,  $\text{Co}_3\text{O}_4$  was fabricated on ITO substrate glass via hydrothermal procedure after annealing in air. The morphology of  $\text{Co}_3\text{O}_4$  can be controlled by adjusting the hydrothermal time. In detail,  $\text{Co}_3\text{O}_4$  nanowires (NWs) can be achieved when the hydrothermal time is 3 h. While the hydrothermal process is stretched to 6 h,  $\text{Co}_3\text{O}_4$  nanolayers (NLS) are obtained. In the reaction process, when putting the ITO substrate into the autoclave, a lot of  $\text{Co}_3\text{O}_4$  precursor nuclei appear on the surface of the substrate. After a 3 h reaction process, nanowires based on the nuclei and the effect of urea appeared, grown with high density on the conductive substrate. With the hydrothermal time increasing to 6 h, the nanowires turned into nanolayers structure. The transformation of the morphology seems to be related to the difference of surface energy. In other words, in order to reduce the surface energy of as-prepared products, the nanowire with large surface will translate into nanolayer structure with relative lower surface energy. Therefore, the formation procedure is an analogous phenomenon in the crystal growth process. Sequentially, Ag nanoparticles (NPs) were prepared by putting the ITO glass which obtained the as-prepared  $\text{Co}_3\text{O}_4$  with different morphologies in the mixed solution containing silver nitrate and sodium citrate. After chemical bath reaction at  $100^\circ\text{C}$  condition, Ag NPs were grown uniformly on the surface of  $\text{Co}_3\text{O}_4$  and  $\text{Co}_3\text{O}_4/\text{Ag}$  composite structure is prepared finally.

The morphology of as-prepared samples was characterized by the typical SEM measurement. Fig. 2(a) and (b) shows a top-view SEM image of  $\text{Co}_3\text{O}_4$  NWs and  $\text{Co}_3\text{O}_4$  NLS, respectively. It is obvious that  $\text{Co}_3\text{O}_4$  NWs and  $\text{Co}_3\text{O}_4$  NLS were uniformly and densely covered on the substrate after the hydrothermal grow process. The surface of both  $\text{Co}_3\text{O}_4$  NWs and  $\text{Co}_3\text{O}_4$  NLS are smooth, and reveal a diameter of 70 nm as well as a thickness of 60 nm. The morphologies of the  $\text{Co}_3\text{O}_4/\text{Ag}$  composite structure were investigated. As shown in Fig. 2(c) and (d), the final products inherit the original morphology of as-prepared  $\text{Co}_3\text{O}_4$  NWs and  $\text{Co}_3\text{O}_4$  NLS. It can be clearly observed that the surface of NWs and NLS appears to be coarse, and many Ag nanoparticles were loaded on the surface of the NWs and NLS core.

Detailed microstructure information of  $\text{Co}_3\text{O}_4/\text{Ag}$  NWs and  $\text{Co}_3\text{O}_4/\text{Ag}$  NLS is investigated through HRTEM measurement accompanied by selected area electron diffraction (SAED). The HRTEM image in Fig. 3(a) shows the distinct lattice fringe of  $\text{Co}_3\text{O}_4/\text{Ag}$  NWs. The fringes spacing is measured to be 0.2359 nm, which corresponded to the (111) lattice spacing of Ag. A typical TEM image of the  $\text{Co}_3\text{O}_4/\text{Ag}$  NLS was shown in Fig. 3(b), revealing that the Ag particles were loaded on the  $\text{Co}_3\text{O}_4$  NL closely. In addition, the SAED of the  $\text{Co}_3\text{O}_4/\text{Ag}$  NLS was also displayed as the inset of Fig. 3(b), implying that the  $\text{Co}_3\text{O}_4$  and Ag are well crystallized. Additionally, the specific surface area of the  $\text{Co}_3\text{O}_4/\text{Ag}$  samples with different morphologies was calculated and the data of  $\text{Co}_3\text{O}_4/\text{Ag}$  NWs and

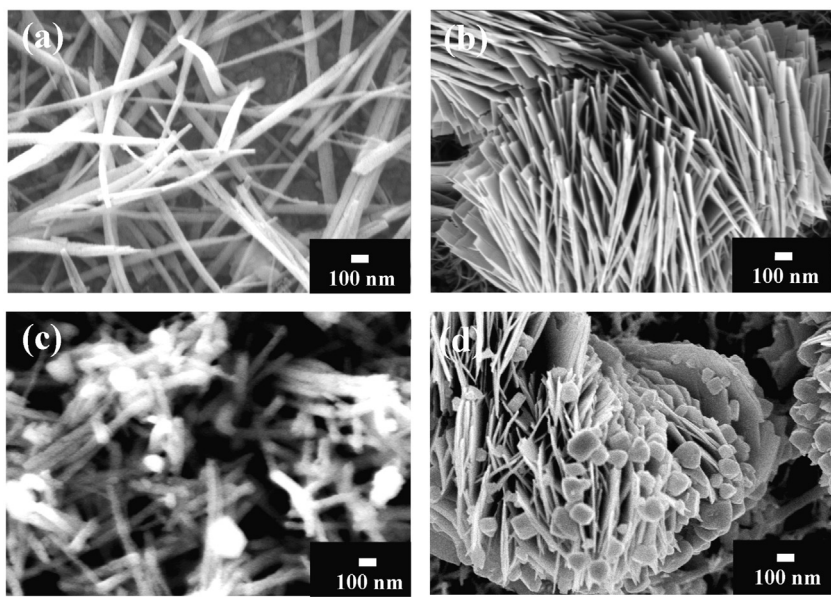


Fig. 2. SEM images of  $\text{Co}_3\text{O}_4$  and  $\text{Co}_3\text{O}_4/\text{Ag}$ : (a)  $\text{Co}_3\text{O}_4$  NWs, (b)  $\text{Co}_3\text{O}_4$  NLS, (c)  $\text{Co}_3\text{O}_4/\text{Ag}$  NWs, (d)  $\text{Co}_3\text{O}_4/\text{Ag}$  NLS.

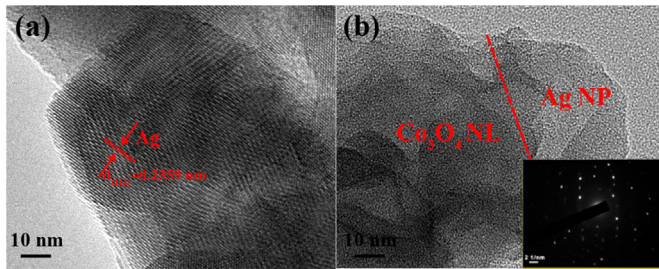


Fig. 3. HRTEM and SAED (inset) images of (a)  $\text{Co}_3\text{O}_4/\text{Ag}$  NWs, (b)  $\text{Co}_3\text{O}_4/\text{Ag}$  NLS.

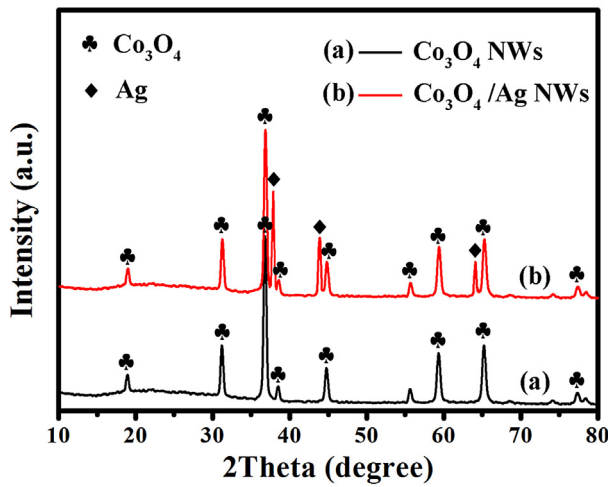


Fig. 4. XRD patterns of (a)  $\text{Co}_3\text{O}_4$  NWs, (b)  $\text{Co}_3\text{O}_4/\text{Ag}$  NWs.

$\text{Co}_3\text{O}_4/\text{Ag}$  NLS was further measured. The surface area of  $\text{Co}_3\text{O}_4/\text{Ag}$  NWs and  $\text{Co}_3\text{O}_4/\text{Ag}$  NLS is  $26 \text{ m}^2 \text{ g}^{-1}$  and  $22 \text{ m}^2 \text{ g}^{-1}$ , respectively.

Fig. 4 gives the XRD patterns of (a)  $\text{Co}_3\text{O}_4$  NWs and (b)  $\text{Co}_3\text{O}_4/\text{Ag}$  NWs, respectively. The corresponding XRD pattern of  $\text{Co}_3\text{O}_4$  NWs is displayed in Fig. 4(a), it can be seen that a set of characteristic peaks are indexed to cubic phase  $\text{Co}_3\text{O}_4$  with the lattice constant  $a = 8.084 \text{ \AA}$ , which is consistent with that of JCPDS Card No. 42-1467. The XRD characterization reveals the crystalline spinel structure

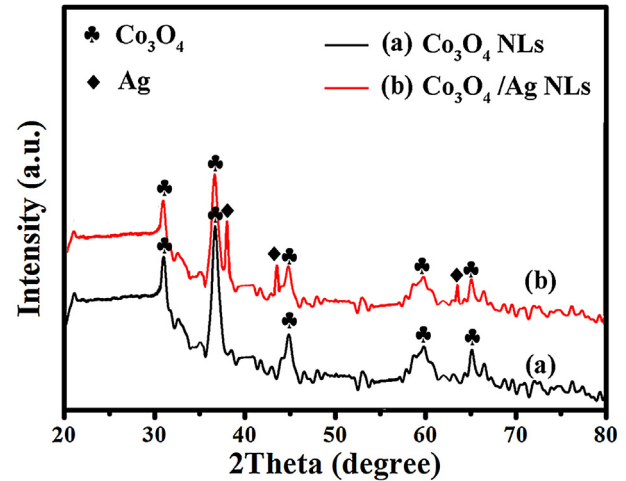
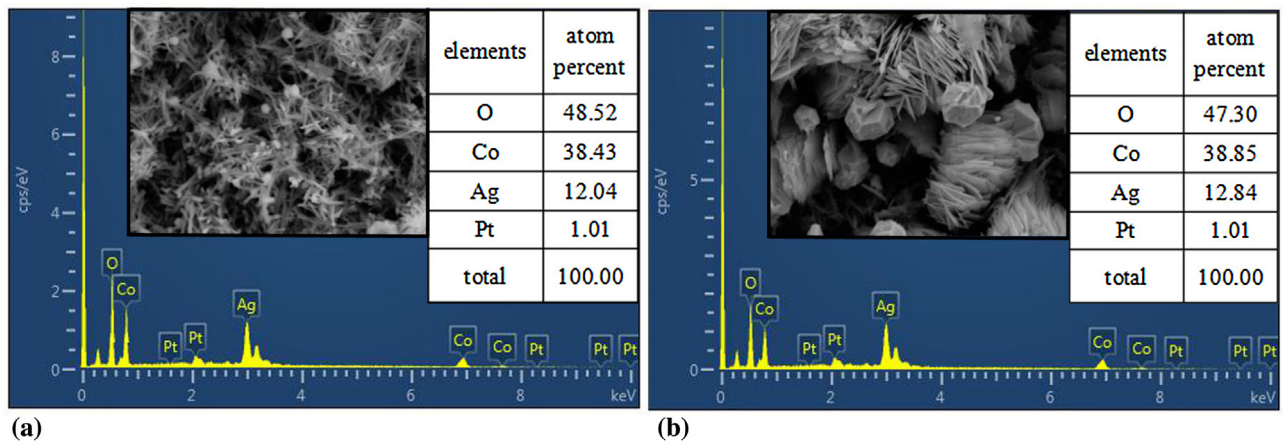
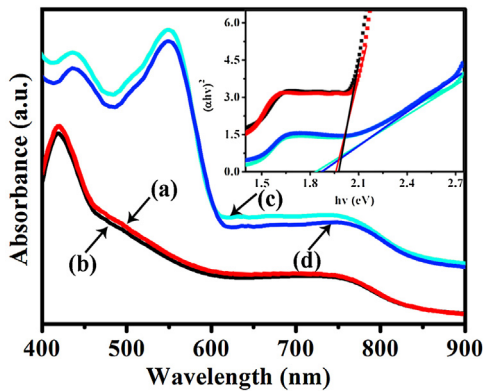


Fig. 5. XRD patterns of (a)  $\text{Co}_3\text{O}_4$  NLS, (b)  $\text{Co}_3\text{O}_4/\text{Ag}$  NLS.

of  $\text{Co}_3\text{O}_4$  NWs with no peaks assignable to other crystal structure phases of cobalt oxides. The corresponding XRD pattern of  $\text{Co}_3\text{O}_4/\text{Ag}$  NWs is shown in Fig. 4(b). After Ag NPs loading onto the  $\text{Co}_3\text{O}_4/\text{Ag}$  NWs, besides the diffraction peaks of  $\text{Co}_3\text{O}_4$ , (111), (200) and (220) with  $2\theta$  values around  $38.11^\circ$ ,  $44.30^\circ$  and  $64.44^\circ$  preferred orientation diffraction peaks appeared, consistent with the crystal planes of metallic silver.

Fig. 5 gives the XRD patterns of (a)  $\text{Co}_3\text{O}_4$  NLS and (b)  $\text{Co}_3\text{O}_4/\text{Ag}$  NLS, respectively. The XRD pattern of  $\text{Co}_3\text{O}_4$  NLS is shown in Fig. 5(a), which is matched well with the standard XRD pattern of JCPDS No. 43-1003. The apparent characteristic peaks exhibited well-crystallized  $\text{Co}_3\text{O}_4$  nanolayers. For the  $\text{Co}_3\text{O}_4/\text{Ag}$  NLS revealed in Fig. 5(b), a series of diffraction peaks of Ag NPs can be observed, exemplifying the Ag NPs were successfully coated on the  $\text{Co}_3\text{O}_4$  NLS.

The chemical stoichiometry and the amount of Ag existed in  $\text{Co}_3\text{O}_4/\text{Ag}$  NWs and  $\text{Co}_3\text{O}_4/\text{Ag}$  NLS were further tested using EDS measurement. As shown in Fig. 6(a), the atomic ratio of Co and O was found to be close to 3:4 and the content of Ag on  $\text{Co}_3\text{O}_4/\text{Ag}$  NWs is approximate to 12.04%. The atomic ratio of Co and O was

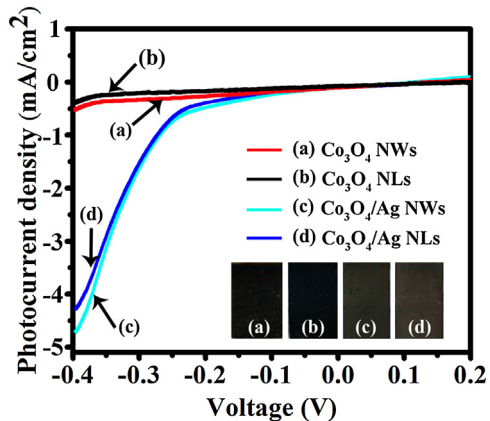
Fig. 6. EDS patterns of (a)  $\text{Co}_3\text{O}_4/\text{Ag}$  NWs and (b)  $\text{Co}_3\text{O}_4/\text{Ag}$  NLs.Fig. 7. UV-vis absorbance spectra and (inset) plot of  $(\alpha h v)^2$  versus  $h v$  of samples of (a)  $\text{Co}_3\text{O}_4$  NWs, (b)  $\text{Co}_3\text{O}_4$  NLs, (c)  $\text{Co}_3\text{O}_4/\text{Ag}$  NWs and (d)  $\text{Co}_3\text{O}_4/\text{Ag}$  NLs, respectively.

also nearly to 3:4 and the content of Ag on  $\text{Co}_3\text{O}_4/\text{Ag}$  NLs is to 12.84% approximately, as shown in Fig. 6(b).

The optical absorbance behavior of the prepared samples: (a)  $\text{Co}_3\text{O}_4$  NWs (b)  $\text{Co}_3\text{O}_4$  NLs (c)  $\text{Co}_3\text{O}_4/\text{Ag}$  NWs and (d)  $\text{Co}_3\text{O}_4/\text{Ag}$  NLs, was studied by UV-vis spectrophotometer in the absorption mode, as is shown in Fig. 7. The data was recorded in the wavelength range of 400–900 nm. Furthermore, Fig. 7(c) and (d) showed a red-shift of  $\text{Co}_3\text{O}_4/\text{Ag}$  composite which by reason of Ag coated on  $\text{Co}_3\text{O}_4$ . From the UV-vis spectrum, the band gap energies can be calculated from the  $(\alpha h v)^2$  versus  $h v$  plot in the inset of Fig. 7, from the intersection of extrapolating the linear portion [29].

$$(\alpha h v)^2 = A(hv - Eg) \quad (1)$$

where  $\alpha$  is absorption coefficient,  $h$  is Planck's constant,  $v$  is frequency and  $A$  is the absorbance. The band gap energy of the  $\text{Co}_3\text{O}_4$  NWs and  $\text{Co}_3\text{O}_4$  NLs were determined through the  $(\alpha h v)^2$  vs.  $h v$  plot, which were shown in Fig. 7(a) and (b). It was observed that the  $\text{Co}_3\text{O}_4$  NWs and  $\text{Co}_3\text{O}_4$  NLs have similar band gap with the values of 1.95 and 1.98 eV achieved via the extrapolation on the x axis. As shown in Fig. 7(c) and (d), the estimated band gap of  $\text{Co}_3\text{O}_4/\text{Ag}$  NWs and  $\text{Co}_3\text{O}_4/\text{Ag}$  NLs are 1.83 and 1.87 eV, respectively, from the extrapolating on the x axis as well. It should be noted that the band gap energy of  $\text{Co}_3\text{O}_4/\text{Ag}$  NWs and  $\text{Co}_3\text{O}_4/\text{Ag}$  NLs are closely matched to the best band gap of the solar cell materials with 1.45 eV. Hence,  $\text{Co}_3\text{O}_4/\text{Ag}$  NWs and  $\text{Co}_3\text{O}_4/\text{Ag}$  NLs, especially the  $\text{Co}_3\text{O}_4/\text{Ag}$  NWs, have the high absorption intensity and indicate the best photoreponse in the visible light region as well water splitting process.

Fig. 8. Photocurrent density-voltage curves of as-prepared (a)  $\text{Co}_3\text{O}_4$  NWs, (b)  $\text{Co}_3\text{O}_4$  NLs, (c)  $\text{Co}_3\text{O}_4/\text{Ag}$  NWs and (d)  $\text{Co}_3\text{O}_4/\text{Ag}$  NLs, respectively.

In order to investigate the PEC performance of  $\text{Co}_3\text{O}_4$  NWs,  $\text{Co}_3\text{O}_4$  NLs,  $\text{Co}_3\text{O}_4/\text{Ag}$  NWs and  $\text{Co}_3\text{O}_4/\text{Ag}$  NLs, respectively, linear-sweep voltammograms measurement for the samples were shown in Fig. 8. The photocurrent densities of  $\text{Co}_3\text{O}_4$  NWs,  $\text{Co}_3\text{O}_4$  NLs,  $\text{Co}_3\text{O}_4/\text{Ag}$  NWs and  $\text{Co}_3\text{O}_4/\text{Ag}$  NLs were  $-0.50 \text{ mA cm}^{-2}$  at  $-0.4 \text{ V}$  versus  $\text{Ag}/\text{AgCl}$ ,  $-0.45 \text{ mA cm}^{-2}$  at  $-0.4 \text{ V}$  versus  $\text{Ag}/\text{AgCl}$ ,  $-4.73 \text{ mA cm}^{-2}$  at  $-0.4 \text{ V}$  versus  $\text{Ag}/\text{AgCl}$  and  $-4.26 \text{ mA cm}^{-2}$  at  $-0.4 \text{ V}$  versus  $\text{Ag}/\text{AgCl}$ . Based on the above results, it can be concluded that the photocurrent densities of  $\text{Co}_3\text{O}_4$  NWs and  $\text{Co}_3\text{O}_4$  NLs are similar and the slight difference of photocurrent density are derived from the different crystalline structures perhaps and morphologies. And the incorporation of Ag particles onto the  $\text{Co}_3\text{O}_4$  leads to an improvement of photocurrent compared with pure  $\text{Co}_3\text{O}_4$ . In particular,  $\text{Co}_3\text{O}_4/\text{Ag}$  NWs present the highest photocurrent density and excellent performance. In general, the geometrical parameter of morphology has some vital effects on the chemical/physical properties, in particular, when the structure is in the nanometer scale. Therefore, the nanoscale dimensions have an important effect on the efficient PEC water splitting process.  $\text{Co}_3\text{O}_4$  NLs as photoelectrode for PEC water splitting ascribed to the morphological properties, including broaden light absorption, large surface area and more surface atoms.  $\text{Co}_3\text{O}_4$  NWs present higher PEC performance than that of  $\text{Co}_3\text{O}_4$  NL, besides the advantages mentioned above, the one dimension structure can also provide high surface-to-volume ratios and the direct charge transport pathways, which lead to the performance differences.

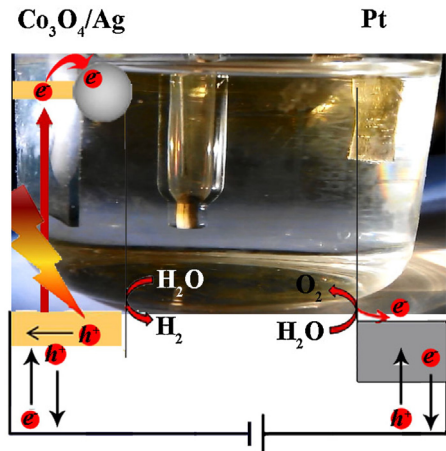


**Fig. 9.** Schematic diagram of the  $\text{Co}_3\text{O}_4/\text{Ag}$  structure electrode and charge-transfer process.

What's more, it is believed that the optimized PEC performance of the  $\text{Co}_3\text{O}_4/\text{Ag}$  structure photocathodes is attributed to the efficiency of light-capturing as well as charge injection and collection process. For the  $\text{Co}_3\text{O}_4/\text{Ag}$  structure, an enhanced efficiency of light-harvesting can be achieved by preparing nanowire and nanolayer structure with unique morphological, electrical, and optoelectronic properties as photocathode. These nanostructures improve light harvesting ability through multiple reflections between nanostructures. Therefore, the light utilization was strengthened by reflecting unabsorbed photons back to nanostructure and utilized once again, which is in favor of the full utilization of incident light. Additionally, Ag NPs loaded on  $\text{Co}_3\text{O}_4$  efficiently increased the surface roughness, which was beneficial to improve the light-harvesting ability. The schematic diagram of the charge-transfer process based on  $\text{Co}_3\text{O}_4/\text{Ag}$  structure was revealed in Fig. 9. The loaded Ag NPs, working as electron traps, can facilitate the separation of photo-induced electron-hole pairs and strengthen the interfacial photo-electrons transfer process [30]. When these  $\text{Co}_3\text{O}_4/\text{Ag}$  composite structures are illuminated by light whose energy is higher than their band gap energy, electron-hole pairs can be generated. Subsequently, the photogenerated electrons are excited to the conduction band of  $\text{Co}_3\text{O}_4$  and then entrapped by Ag NPs because of its high Schottky barriers existing at the metal-semiconductor interface. In detail, the Schottky barrier served as a trap for electrons was generated is attributed to the different function of Ag and  $\text{Co}_3\text{O}_4$ , and the formation of Schottky barrier facilitate the photogenerated electrons migrating from Ag NPs to  $\text{Co}_3\text{O}_4$  surface. That is, the Ag NPs function as an electron sink to harvest photo-induced electrons from  $\text{Co}_3\text{O}_4$ , meanwhile act as a reduction active site to reduce  $\text{H}_2\text{O}$  efficiently. Therefore, the transportation of charge has been accelerated and the recombination of electrons-holes has been indeed inhibited. In the PEC measurement, the electrons on the surface of Ag NPs have been exhausted by  $\text{H}^+$ , meanwhile, the holes can flow into the ITO conductive substrate and transfer to the counter electrode via an external circuit. In addition, low-dimensional (one and two dimensional with thin in depth) nanostructure can offer a high hole transfer rate and suppress the recombination rate of photogenerated electron-hole pairs, especially the one-dimensional structure of  $\text{Co}_3\text{O}_4$  provide a direct pathway for holes, which means the  $\text{Co}_3\text{O}_4$  NWs and  $\text{Co}_3\text{O}_4/\text{Ag}$  NWs present superior PEC performance than that of  $\text{Co}_3\text{O}_4$  NLS and  $\text{Co}_3\text{O}_4/\text{Ag}$  NLS, respectively.

Incident photo-to-current conversion efficiency (IPCE) tests were conducted to research the relationship between light absorption and photocurrent based on various photoelectrodes of  $\text{Co}_3\text{O}_4$  and  $\text{Co}_3\text{O}_4/\text{Ag}$ . The IPCE values were measured and presented in

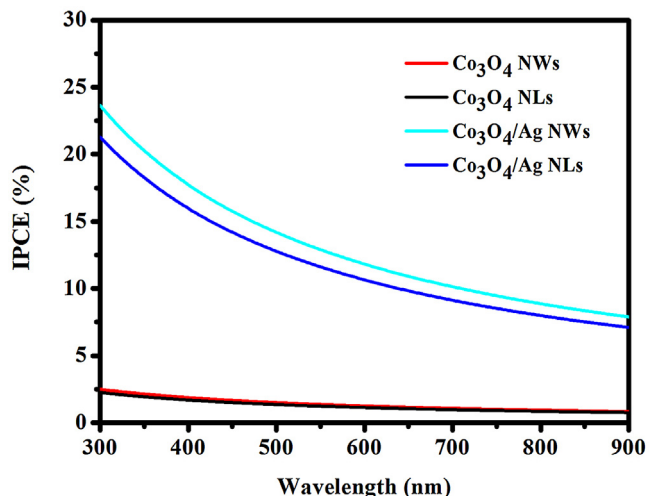


**Fig. 10.** IPCE plots in the range of 300–900 nm at  $-0.4$  V vs. Ag/AgCl of as-prepared  $\text{Co}_3\text{O}_4$  NWs,  $\text{Co}_3\text{O}_4$  NLSs,  $\text{Co}_3\text{O}_4/\text{Ag}$  NWs and  $\text{Co}_3\text{O}_4/\text{Ag}$  NLSs, respectively.

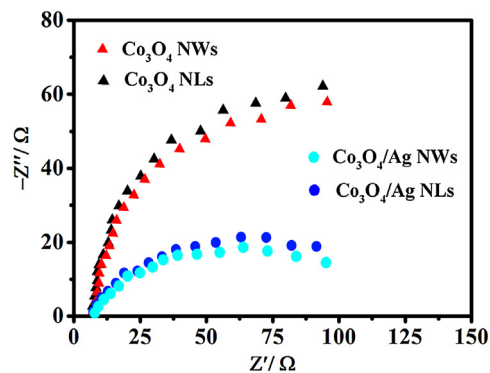


**Fig. 11.** Electrochemical impedance spectroscopy of as-prepared  $\text{Co}_3\text{O}_4$  NWs,  $\text{Co}_3\text{O}_4$  NLSs,  $\text{Co}_3\text{O}_4/\text{Ag}$  NWs and  $\text{Co}_3\text{O}_4/\text{Ag}$  NLSs, respectively.

**Fig. 10.** It can be observed that the IPCE profile of the  $\text{Co}_3\text{O}_4/\text{Ag}$  NWs and  $\text{Co}_3\text{O}_4/\text{Ag}$  NLSs is broadened and strengthened over the visible light region compared with that of  $\text{Co}_3\text{O}_4$  NWs and  $\text{Co}_3\text{O}_4$  NLSs, which means the  $\text{Co}_3\text{O}_4/\text{Ag}$  NWs and  $\text{Co}_3\text{O}_4/\text{Ag}$  NLSs present a higher quantum efficiency than that of  $\text{Co}_3\text{O}_4$  NWs and  $\text{Co}_3\text{O}_4$  NLSs.

In order to investigate the charge transport behavior of as-prepared samples, electrochemical impedance spectroscopy (EIS) was characterized by electrochemical workstation. Fig. 11 shows the Nyquist plots from the EIS measurement of the  $\text{Co}_3\text{O}_4$  and  $\text{Co}_3\text{O}_4/\text{Ag}$  electrodes. In each case, a depressed semicircle can be measured and the radius is related with charge transfer resistance. The sample with smaller arc radius implies that it has faster interfacial electron transfer and longer lifetime of photo-induced electron-hole pairs. Here, it can be seen that the decrease of interfacial resistance of  $\text{Co}_3\text{O}_4/\text{Ag}$  electrodes is consistent with the increase in current density revealed in Fig. 8. The plots show further decrease in the charge transfer resistance at the semiconductor-electrolyte interface of  $\text{Co}_3\text{O}_4$  upon coating of Ag NPs that allows the tunneling of photo-generated electrons to the electrode surface for water reduction while inhibiting the back recombination with photo-generated holes on the  $\text{Co}_3\text{O}_4$  surface.

The PEC performance and stability of  $\text{Co}_3\text{O}_4$  and  $\text{Co}_3\text{O}_4/\text{Ag}$  photocathodes was further tested under on/off cycle illumination condition at  $-0.4$  V versus Ag/AgCl. As shown in Fig. 12, the photocurrent densities of the  $\text{Co}_3\text{O}_4/\text{Ag}$  NWs and  $\text{Co}_3\text{O}_4/\text{Ag}$  NLSs were  $-4.73 \text{ mA cm}^{-2}$  and  $-4.26 \text{ mA cm}^{-2}$ , respectively. The improved photocurrent of  $\text{Co}_3\text{O}_4/\text{Ag}$  NWs and  $\text{Co}_3\text{O}_4/\text{Ag}$  NLSs are more than 9

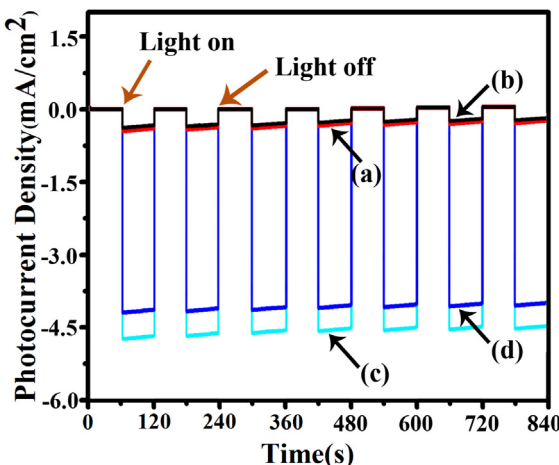


**Fig. 12.** Photocurrent density-time curves under illumination with 60 s light on/off cycles of as-prepared (a)  $\text{Co}_3\text{O}_4$  NWs, (b)  $\text{Co}_3\text{O}_4$  NLs, (c)  $\text{Co}_3\text{O}_4/\text{Ag}$  NWs and (d)  $\text{Co}_3\text{O}_4/\text{Ag}$  NLs, respectively.

times as much of that of the pure  $\text{Co}_3\text{O}_4$  NWs and  $\text{Co}_3\text{O}_4$  NLs, which is consistent with Fig. 8. In addition, it can be observed clearly that the current values of  $\text{Co}_3\text{O}_4/\text{Ag}$  NWs and  $\text{Co}_3\text{O}_4/\text{Ag}$  NLs have no obvious decrease in the light-on period of each cycle, indicating that the photocurrent density-time patterns of light on/off cycles are reproducible and stable of the  $\text{Co}_3\text{O}_4/\text{Ag}$  photocathodes.

#### 4. Conclusion

$\text{Co}_3\text{O}_4$  with different morphologies of nanowire and nanolayer were fabricated on ITO conductive substrate successfully and served as photocathode material for efficient PEC water splitting for the first time. In order to achieve an improved PEC performance, noble metal Ag particles were loaded onto the  $\text{Co}_3\text{O}_4$  after hydrothermal process, and  $\text{Co}_3\text{O}_4/\text{Ag}$  composite structure was obtained. The measurement result shows that  $\text{Co}_3\text{O}_4$  NWs and  $\text{Co}_3\text{O}_4$  NLs exhibit similar PEC property, while a significantly improved PEC activity was obtained of  $\text{Co}_3\text{O}_4/\text{Ag}$  composite structure that after depositing Ag NPs, the photocurrent densities were up to  $-4.26 \text{ mA cm}^{-2}$  and  $-4.73 \text{ mA cm}^{-2}$ , respectively. The excellent PEC performance of  $\text{Co}_3\text{O}_4/\text{Ag}$  composite structure can be ascribed to high light capture efficiency, a widened photoresponse range, rapid holes mobility and increased interfacial photoelectrons transfer of Ag NPs, which enhances the efficient separation of charge and suppress the recombination of electron-hole pairs. In special,  $\text{Co}_3\text{O}_4/\text{Ag}$  NWs composite exhibits a superior performance than others due to higher holes mobility via the direct electrical pathways. Such high-efficiency  $\text{Co}_3\text{O}_4$  modified with noble metal photoelectrodes should be suitable for other p-type PEC application including tandem p/n-type devices and photovoltaic solar cells in general.

#### Acknowledgements

The authors gratefully acknowledge financial support from National Nature Science Foundation of China (51102174), State Key Laboratory of Heavy Oil Processing (No. SKLHOP201505) and Natural Science Foundation of Tianjin (16JCYBJC17900).

#### References

- [1] T. Hisatomi, J. Kubota, K. Domen, Recent advances in semiconductors for photocatalytic and photoelectrochemical water splitting, *Chem. Soc. Rev.* 43 (2014) 7520–7535.
- [2] N.S. Lewis, D.G. Nocera, Powering the planet: chemical challenges in solar energy utilization, *Proc. Natl. Acad. Sci.* 103 (2006) 15729–15735.
- [3] K. Maeda, K. Domen, Photocatalytic water splitting: recent progress and future challenges, *J. Phys. Chem. Lett.* 1 (2010) 2655–2661.
- [4] A. Kudo, Y. Misaki, Heterogeneous photocatalyst materials for water splitting, *Chem. Soc. Rev.* 38 (2009) 253–278.
- [5] M.G. Walter, E.L. Warren, J.R. McKone, S.W. Boettcher, Q. Mi, E.A. Santori, N.S. Lewis, Solar water splitting cells, *Chem. Rev.* 110 (2010) 6446–6473.
- [6] A. Fujishima, K. Honda, Electrochemical photolysis of water at a semiconductor electrode, *Nature* 238 (1972) 37–38.
- [7] T. Wang, Z.B. Luo, C.C. Li, J.L. Gong, Controllable fabrication of nanostructured materials for photoelectrochemical water splitting via atomic layer deposition, *Chem. Soc. Rev.* 43 (2014) 7469–7484.
- [8] F.E. Osterloh, Inorganic nanostructures for photoelectrochemical and photocatalytic water splitting, *Chem. Soc. Rev.* 42 (2013) 2294–2320.
- [9] T.T. Hong, Z.F. Liu, H. Liu, J.Q. Liu, X.Q. Zhang, J.H. Han, K.Y. Guo, B. Wang, Preparation and enhanced photoelectrochemical performance of selenite-sensitized zinc oxide core/shell composite structure, *J. Mater. Chem. A* 3 (2015) 4239–4247.
- [10] J.H. Han, Z.F. Liu, K.Y. Guo, B. Wang, X.Q. Zhang, T.T. Hong, High-efficiency photoelectrochemical electrodes based on  $\text{ZnIn}_2\text{S}_4$  sensitized  $\text{ZnO}$  nanotube arrays, *Appl. Catal. B Environ.* 163 (2015) 179–188.
- [11] J.H. Han, Z.F. Liu, B. Yadian, Y.Z. Huang, K.Y. Guo, Z.C. Liu, B. Wang, Y.J. Li, T. Cui, Synthesis of metal sulfide sensitized zinc oxide-based core/shell/shell nanorods and their photoelectrochemical properties, *J. Power Sources* 268 (2014) 388–396.
- [12] Z.F. Liu, K.Y. Guo, J.H. Han, Y.J. Li, T. Cui, B. Wang, J. Ya, C.L. Zhou, Dendritic  $\text{TiO}_2/\text{In}_2\text{S}_3/\text{AgInS}_2$  trilaminar core-shell branched nanoarrays and the enhanced activity for photoelectrochemical water splitting, *Small* 10 (2014) 3153–3161.
- [13] J. Zhang, Z. Liu, Z. Liu, Novel  $\text{WO}_3/\text{Sb}_2\text{S}_3$  heterojunction photocatalyst based on  $\text{WO}_3$  of different morphologies for enhanced efficiency in photoelectrochemical water splitting, *ACS Appl. Mater. Interfaces* 8 (2016) 9684–9691.
- [14] Y. Mao, W. Li, P. Liu, J. Chen, E.J. Liang, Topotactic transformation to mesoporous  $\text{Co}_3\text{O}_4$  nanosheet photocathode for visible-light-driven direct photoelectrochemical hydrogen generation, *Mater. Lett.* 134 (2014) 276–280.
- [15] X. Wang, H. Guan, S.M. Chen, H.Q. Li, T.Y. Zhai, D.M. Tang, Y. Bando, D. Golberg, Self-stacked  $\text{Co}_3\text{O}_4$  nanosheets for high-performance lithium ion batteries, *Chem. Commun.* 47 (2011) 12280–12282.
- [16] Q. Hao, Y. Yu, D.Y. Zhao, C.X. Xu, Composited  $\text{Co}_3\text{O}_4/\text{Ag}$  with flower-like nanosheets anchored on a porous substrate as a high-performance anode for Li-ion batteries, *J. Mater. Chem. A* 3 (2015) 15944–15950.
- [17] C. Yuan, L. Yang, L. Hou, X. Zhang, X.W. Lou, Growth of ultrathin mesoporous  $\text{Co}_3\text{O}_4$  nanosheet arrays on Ni foam for high-performance electrochemical capacitors, *Energy Environ. Sci.* 5 (2012) 7883–7887.
- [18] X.H. Wang, X.X. Wu, B.G. Xu, T. Hua, Coralloid and hierarchical  $\text{Co}_3\text{O}_4$  nanostructures used as supercapacitors with good cycling stability, *J. Solid State Electrochem.* 20 (2016) 1303–1309.
- [19] H. Nguyen, S.A. ElSafty, Meso- and macroporous  $\text{Co}_3\text{O}_4$  nanorods for effective VOC gas sensors, *J. Phys. Chem. C* 115 (2011) 8466–8474.
- [20] Q. Shen, Z.F. Chen, X.F. Huang, M.C. Liu, G.H. Zhao, High-yield and selective photoelectrocatalytic reduction of  $\text{CO}_2$  to formate by metallic copper decorated  $\text{Co}_3\text{O}_4$  nanotube arrays, *Environ. Sci. Technol.* 49 (2015) 5828–5835.
- [21] L. Xu, Q.Q. Jiang, Z.H. Xiao, X.Y. Li, J. Huo, S.Y. Wang, L.M. Dai, Plasma-engraved  $\text{Co}_3\text{O}_4$  nanosheets with oxygen vacancies and high surface area for the oxygen evolution reaction, *Angew. Chem.* 128 (2016) 5363–5367.
- [22] T. Sreethawong, S. Yoshikawa, Comparative investigation on photocatalytic hydrogen evolution over Cu-, Pd-, and Au-loaded mesoporous  $\text{TiO}_2$  photocatalysts, *Catal. Commun.* 6 (2005) 661–668.
- [23] Z.B. Zhuang, W.C. Sheng, Y.S. Yan, Synthesis of monodispere  $\text{Au}@\text{Co}_3\text{O}_4$  core-shell nanocrystals and their enhanced catalytic activity for oxygen evolution reaction, *Adv. Mater.* 26 (2014) 3950–3955.
- [24] G.M. Suppes, P.J. Fortin, S. Holdcroft, Photoelectrochemical hydrogen evolution: single-layer, conjugated polymer films bearing surface-deposited Pt nanoparticles, *J. Electrochem. Soc.* 162 (2015) 551–556.
- [25] L. Xu, Z.Y. Yin, S.W. Cao, Z.X. Fan, X. Zhang, H. Zhang, C. Xue, Rational synthesis of triangular  $\text{Au}-\text{Ag}_2\text{S}$  hybrid nanoframes with effective photoresponses, *Chem. A Eur. J.* 20 (2014) 2742–2745.
- [26] P. Wang, Y. Xia, P.P. Wu, X.F. Wang, H.G. Yu, J.G. Yu, Cu(II) as a general cocatalyst for improved visible-light photocatalytic performance of photosensitive Ag-based compounds, *J. Phys. Chem. C* 118 (2014) 8891–8898.
- [27] J. Wang, F.E. Osterloh, Limiting factors for photochemical charge separation in  $\text{BiVO}_4/\text{Co}_3\text{O}_4$ , a highly active photocatalyst for water oxidation in sunlight, *J. Mater. Chem. A* 2 (2014) 9405–9411.
- [28] L.J. Zhou, Y. Zou, G.D. Li, X. Zou, M. Fan, Y. Liu, Facile precursor-mediated synthesis of porous core-shell-type  $\text{Co}_3\text{O}_4$  octahedra with large surface area for photochemical water oxidation, *RSC Adv.* 4 (2014) 22951–22954.
- [29] H.T. Yu, X. Quan, Y.B. Zhang, N. Ma, S. Chen, H.M. Zhao, Electrochemically assisted photocatalytic inactivation of *Escherichia coli* under visible light using a  $\text{ZnIn}_2\text{S}_4$  film electrode, *Langmuir* 24 (2008) 7599–7604.
- [30] L. Ge, C.C. Han, J. Liu, Y.F. Li, Enhanced visible light photocatalytic activity of novel polymeric g-C<sub>3</sub>N<sub>4</sub> loaded with Ag nanoparticles, *Appl. Catal. A Gen.* 409–410 (2011) 215–222.